JOINT EUROPEAN TORUS

JET–P(90)06

M.F.F. Nave and J.A. Wesson

Mode Locking in Tokamaks

Mode Locking in Tokamaks

M.F.F. Nave[1] and J.A. Wesson

JET-Joint Undertaking, Culham Science Centre, OX14 3DB, Abingdon, UK

[1]Laboratorio Nacional de Engenharia & Tecnologia Industrial, Sacavem, Portugal

Preprint of Paper to be submitted for publication in
Nuclear Fusion

MODE LOCKING IN TOKAMAKS

M.F.F. Nave* and J.A. Wesson

JET Joint Undertaking, Abingdon, Oxon, England
*Laboratorio Nacional de Engenharia & Tecnologia Industrial,
Sacavem, Portugal

ABSTRACT

The theory of non-linear tearing modes has been extended to include the effects of rotation and interaction with a resistive wall. The time dependent solution of the resulting equations shows a spatial locking of the mode similar to that observed in tokamak experiments. Time dependent numerical calculations show that the model can explain in a qualitative way the overall frequency evolution of mode locking and the radial magnetic field behaviour observed on JET.

1. INTRODUCTION

It is observed that mhd modes in tokamaks exhibit a reduction in frequency as they grow to large amplitudes. In the case of disruption precursors, for example, the frequency can be reduced to zero. This process is called mode locking. The theoretical interpretation of this behaviour in terms of an electromagnetic interaction with conductors surrounding the plasma was proposed in a brief conference paper [1]. We give here a somewhat extended account of the theory and the calculations involved. A description of the experimental results on JET was given by Snipes et al. [2,3].

The growth of tearing modes with their associated magnetic islands leads to helical magnetic field perturbations, $\underline{\tilde{B}}$, outside the plasma. These perturbations are observed to rotate with a frequency typically $\sim$ 1-10kHz. Thus at an external conductor these magnetic perturbations are oscillatory

and the induced electric fields produce fluctuating currents, $\tilde{j}$.

The induced currents give rise to a force $\tilde{j}\times\underline{\tilde{B}}$ in the conductor. Similar $\tilde{j}\times\underline{\tilde{B}}$ forces arise in the plasma and the result is a transfer of momentum from the plasma to the conductor. This causes a slowing of the plasma and a reduction in the frequency. This leads in turn to an increased penetration of the fields into the conductor and to a strengthening of the interaction. The consequence is an increasingly rapid transfer of momentum from the plasma, which finally brings the magnetic islands to rest. The final position of the locked mode depends upon the small scale lack of symmetry of external conductors.

If a tearing-mode unstable configuration is created on a timescale short compared to the non-linear growth time, a magnetic island will start to grow and, according to Rutherford's theory [4],

$$\frac{dw}{dt} = \frac{\eta}{\mu_o}\,\Delta'(0)$$

where w is the island width, η the resistivity and $\Delta'(0)$ is the jump in the logarithmic derivative of the perturbed helical flux function, ψ, across the resonant surface. Thus initially $w \propto t$. Now the magnetic perturbation $\tilde{B}$ is proportional to w^2, and so the force on the plasma $F_p \propto \tilde{B}^2 \propto t^4$. This causes a rapidly increasing deceleration of motion of the magnetic island. There are then two possibilities. In the first, which is generally the case in JET [2], the magnetic islands are brought to rest before they are saturated in amplitude. The growth to saturation then proceeds at zero frequency. The other possibility is that the deceleration is sufficiently slow that saturation occurs first and the deceleration to zero velocity then occurs with an essentially constant value of the magnetic field perturbat-

ion. In both cases the mode is brought to locking by what might be thought of as a magnetic viscous drag in the external conductor.

In the non-linear stage of tearing mode growth the effective Δ' reduces with increasing island width and consequently the dependency of F_p on time is more complicated than outlined above. Furthermore, the transfer of momentum to the plasma depends on the type of rotation, toroidal or poloidal, and on the fraction of the mass involved. These details do not change the overall physics described but will alter the frequency evolution and the time the mode takes to lock [1].

One other matter of interest is the influence of a conducting vessel on the growth of the instability. It is easily seen that there will be a stabilising effect at high frequencies when the vessel behaves as a good conductor. However, as the frequency falls the mode will grow more rapidly and this in turn accelerates the fall in frequency. Thus the island growth and frequency fall drive each other. However, the essential point to recognise is that even a perfectly conducting vessel only has a significant stabilising effect if the resonant surface is in the outer part of the plasma. With a deeper resonance the physics of mode-locking is as described above but the island growth is essentially unaffected by the conducting vessel.

In the following sections we present a theoretical model for non-linear island growth and frequency evolution in the presence of a thin conducting vessel. The model uses the large aspect-ratio approximation and assumes that the plasma mass involved in the rotation is fixed. We then give numerical calculations illustrating the locking of the modes.

2. THEORETICAL MODEL

We consider a circular cross section plasma with minor radius a and

major radius R, surrounded by a thin vessel of radius b, thickness δ and conductivity σ (Fig. 1). For a large aspect-ratio tokamak the equation governing the magnetic perturbations due to a tearing mode is [5]

$$\frac{1}{r}\frac{d}{dr}\,r\,\frac{d\psi}{dr} - \frac{m^2}{r^2}\,\psi - \frac{\mu_o\, dj/dr}{B_\theta(1 - nq/m)}\,\psi = 0 \qquad (1)$$

where j is the toroidal current density, $q(= rB_\phi/RB_\theta)$ is the safety factor, B_ϕ and B_θ being the toroidal and poloidal magnetic fields, n and m are the toroidal and poloidal mode numbers and ψ is the helical flux function with $\tilde{B}_r = (1/r)\partial\psi/\partial\theta$ and $\tilde{B}_\theta = -\partial\psi/\partial r$. The solutions of Eq. (1) give the growth of the magnetic island through [4,6]

$$\frac{dw}{dt} = \frac{\eta}{\mu_o}\,\Delta'(w) \qquad \text{where} \qquad \Delta'(w) = \frac{\psi'}{\psi}\Bigg|_{r_s-w/2}^{r_s+w/2}, \qquad (2)$$

η is the resistivity at the resonant surface ($r = r_s$), and the island width is related to the magnetic perturbation through [4,6]

$$w = 4\left(q|\psi|/q'B_\theta\right)^{1/2}_{r=r_s} \qquad (3)$$

The boundary conditions for equation (1) at the surface of the plasma are obtained by solving the equations for ψ in the outside regions, that is in the vacuum

$$\frac{1}{r}\frac{d}{dr}\,r\,\frac{d\psi}{dr} = \frac{m^2}{r^2}\,\psi$$

and in the vessel

$$\frac{1}{r}\frac{d}{dr}\, r\, \frac{d\psi}{dr} = \left[\frac{m^2}{r^2} - i\omega\mu_o\sigma\right]\, \psi .$$

where ω is the frequency. Finally we take $\psi(\infty) = 0$. Thus, applying the continuity conditions at the interfaces between the regions leads to the boundary condition at the surface of the plasma

$$\left[\frac{\psi'}{\psi}\right]_{r=a} = -\frac{m}{a}\,\frac{1 + f(a/b)^{2m}}{1 - f(a/b)^{2m}}\,, \qquad (4a)$$

where, by taking $\delta/b \ll 1/\omega\tau_v$, where $\tau_v (= \mu_o \sigma b \delta/2)$ is the characteristic resistive time constant of the shell, f is of the form

$$f = \frac{1}{1 + (im/\omega\tau_v)} \qquad (4b)$$

A plot of f as a function of $\omega\tau_v$ for m = 2, is shown in figure (2). For $\omega\tau_v \to \infty$ we have f = 1 as for a perfectly conducting vessel, while for $\omega\tau_v \to 0$ we have f = 0 corresponding to the case of no wall. The subscripts I and R in Fig. 2, and throughout this paper, refer to the imaginary and the real parts respectively.

The force on the plasma caused by the perturbations produces a change of velocity which reduces the frequency seen by the wall. The precise way in which this occurs depends on the details of the plasma response. For purposes of illustration it is assumed that a fixed mass of plasma is involved. The change in the observed frequency is then given by the equation

$$\frac{d\omega}{dt} = \frac{m\int F_\theta r dV}{\int \rho r^2 dV} + \frac{n\int F_\phi dV}{R\int \rho dV} \qquad (5)$$

where ρ is the density of the plasma involved in the rotation and F_θ and F_ϕ are the poloidal and toroidal components of the force perpendicular to the perturbation helix given, in the large aspect ratio approximation, by

$$F_\theta = \tilde{j}\tilde{B}_r = -\frac{1}{\mu_o}\nabla^2\psi\,\frac{1}{r}\,\frac{\partial\psi}{\partial\theta} \qquad (6a)$$

$$F_\phi = \frac{B_\theta}{B_\phi}\,\tilde{j}\tilde{B}_r = -\frac{1}{\mu_o}\nabla^2\psi\,\frac{n}{mR}\,\frac{\partial\psi}{\partial\theta}\ , \qquad (6a)$$

where $\tilde{j}$ is the helical perturbed current.

Substitution of equations (6) into equation (5) leads to

$$\frac{d\omega}{dt} = \frac{aJ}{2\mu_o}\,Im(\psi^*\psi')_{r=a} \qquad \text{where} \quad J = \frac{m^2}{\int\rho r^3 dr} + \frac{n^2}{R^2\int\rho r dr}\ . \qquad (7)$$

The first term in J is much larger than the second but it is possible that in some circumstances the poloidal motion is prevented by damping. In this case the first term in J is removed.

The complete time evolution is described by equations (1)-(4) and (7), and the resulting solutions are described in the following two sections.

3. ANALYTIC APPROXIMATIONS FOR MODE LOCKING

The right hand side of Eq.(7) is a function of both the frequency and the island width. The frequency dependence appears in the term $Im(\psi^*\,\psi')$ through the parameter f in the boundary condition given by Eqs. (4a) and (4b). The dependence on the island width arises from Eq. (3), which gives $|\psi|^2 \propto w^4$, and from the mass involved in the calculation of the inertia, leading to $d\omega/dt \propto w^4$ when the whole plasma rotates and $d\omega/dt \propto w^3$ if only the plasma in the island rotates. The evolution of the frequency is

therefore coupled to the evolution of the island width, given by the solution of Eq. (2).

In order to gain further physical insight when deriving analytical expressions, and also to facilitate the numerical task of determining ψ, it is convenient to express ψ in the resistive wall problem as a linear combination of two solutions for a perfectly conducting wall. We therefore express ψ as

$$\psi = \psi_\infty + \alpha \ (\psi_v - \psi_\infty) \tag{8}$$

where ψ_v is the solution for a perfectly conducting vessel at r = b (that is f = 1) and ψ_∞ is the solution for no wall (that is $b \to \infty$ or f = 0). The dependency on the frequency and wall resistivity appears only in the parameter α, which is determined from the boundary condition (4a) as

$$\alpha = \frac{f}{f - s(f - 1)} \tag{9}$$

where

$$s = \frac{1}{1 - (a/b)^{2m}} \ \frac{\psi_v(a)}{\psi_\infty(a)} \ .$$

We choose ψ_v and ψ_∞ to be real, though α is in general complex through the parameter f.

After some algebra Eqs. (8) and (9) give

$$Im(\psi^*\psi')_{r=a} = 2 \frac{m}{a} \psi_\infty^2(a) \left(\frac{a}{b}\right)^{2m} s \ Im(\alpha)_{r=a}.$$

Thus, Eq. (7) can be rewritten as

$$\frac{d\omega}{dt} = \frac{mJ}{\mu_o}\,\psi_\infty^2(r_s)\,(r_s/b)^{2m}\,g\,f_I \qquad (10)$$

where

$$g = \left(\frac{a}{r_s}\right)^{2m}\left(\frac{\psi_\infty(a)}{\psi_\infty(r_s)}\right)^2 \frac{s}{|f - s(f-1)|^2}$$

is a factor of 0(1) depending on the particular equilibrium and varying with the frequency.*

In general ψ_v and ψ_∞ need to be determined numerically. However, an analytical expression for g can be obtained in the case when the current density is small in the outer region of the plasma. Then the solutions for ψ_v and ψ_∞ for $r > r_s$ take the form r^m and r^{-m}, and g becomes

$$g = \frac{1 - (r_s/b)^{2m}}{|1 - f(r_s/b)^{2m}|^2}\,. \qquad (11)$$

In the case of $(r_s/b)^{2m} \ll 1$, g tends to unity and only the imaginary part of f appears in the equation for dω/dt. It is clear from Fig.2, that most of the frequency decay would then occur when $\omega\tau_v \sim m$, where f_I has a maximum.

The full non-linear problem requires numerical solutions. However the basic features of the evolution of the frequency can be illustrated by the following calculation.

The island growth is given by Eq.(2), where the dependence of Δ' on w is normally monotonically decreasing. Here we will use the approximation

---

*Berge et al. [7] obtain a different form for dω/dt and state that our derivation is in error. In fact this is not so. In their paper $\mathrm{Im}(\psi^*\psi')_a$ was written as $|\psi_a|^2\,\mathrm{Im}(\psi'/\psi)_a$ and then, in Section 4, they take the frequency dependence to be given by $\mathrm{Im}(\psi'/\psi)_a$. To obtain the correct result with this formulation it is necessary to include the frequency dependence of $|\psi_a|^2$. The result obtained then, is the same as ours.

$$\Delta'(w) = \Delta'(0)(1 - w/w_s)$$

where w_s is the saturated island size, giving the solution

$$w = w_s(1 - \exp(-t/\tau_s)), \quad \text{where} \quad \tau_s = \mu_o w_s/\eta\Delta'(0) \tag{12}$$

To calculate the time development of the frequency we consider the case of toroidal rotation. We assume the gradient of the current density to be small in the outer region of the plasma and $(r_s/b)^{2m} << 1$. Then, using Eqs. (3), (10) and (11) we obtain

$$\frac{dw}{dt} = - c \frac{1}{\tau_A^2} \frac{w\tau_v}{w^2\tau_v^2 + m^2} \left(\frac{w}{a}\right)^4 \tag{13}$$

where

$$c = \frac{m^2}{256} \left(\frac{r_s}{b}\right)^{2m} \left(\frac{aq'}{q}\right)^2_{r_s} \qquad \text{and} \qquad \tau_A^2 = \mu_o/Ja^2B_\theta^2(r_s)$$

In the case where locking occurs before saturation, the solution for w given by Eq. (12) can be expanded to give

$$w = w_s t/\tau_s$$

and the solution of Eq. (13) is then

$$(\omega_o^2 - \omega^2)\ \tau_v^2 - 2m^2 \ln \frac{\omega}{\omega_o} = \alpha \frac{\tau_v t^5}{\tau_A^2 \tau_s^4} \tag{14}$$

where

$$\alpha = \frac{2}{5} c \left(\frac{w_s}{a}\right)^4$$

Equations (12) and (14) show the basic features of mode-locking. The island grows to saturation on a timescale determined by the resistivity of the plasma and the strength of the instability. The frequency change described by Eq. (13) occurs in two phases. In the first phase the first term on the left of Eq. (14) dominates. During this phase the t^5 dependence means that the change in frequency is slow initially but becomes increasingly rapid after a time characterised by

$$\tau_L = (\omega_o^2 \tau_v \tau_A^2 \tau_s^4/\alpha)^{1/5}.$$

In the final phase of the locking the second term in Eq.(14) dominates and the residual frequency decays as $\exp-(t/\tau_D)^5$ with

$$\tau_D = (2m^2 \tau_v^{-1} \tau_A^2 \tau_s^4/\alpha)^{1/5}$$

In the above calculation we have assumed that the whole plasma moves toroidally. To estimate the effect of taking a different mass and direction of rotation, we again consider Eq. (13), rewritten as

$$\frac{d\omega}{dt} = -\frac{1}{C}\frac{1}{\tilde{\tau}_A^2}\frac{\omega\tau_v}{\omega^2\tau_v^2 + m^2},$$

where now we define

$$\tilde{\tau}_A^2 = \frac{a^2}{\tilde{B}_\theta^2/\mu_o\bar{\rho}} \quad \text{and} \quad C = \frac{1}{(a/b)^{2m} a^4 \bar{\rho}}\left(\frac{m^2}{\int \rho r^3 dr} + \frac{n^2}{R^2 \int \rho r dr}\right)^{-1}.$$

where $\bar{\rho} = \frac{2}{a^2}\int \rho r dr$.

We now calculate C by taking separately the cases of poloidal and toroidal rotation, that is by retaining either the first or the second term in the denominator of C. Then for a parabolic density profile, the values of C for m = 2, n = 1 with b = a are as given in Table 1.

	Poloidal Rotation	Toroidal Rotation
Full plasma	$\frac{1}{24}$	$\frac{1}{2}\frac{R^2}{a^2}$
Island only	$\sim \frac{1}{2}\frac{wr_s^3}{a^4}$	$\sim 2\frac{wr_sR^2}{a^4}$

Table 1

Thus, the constant C for toroidal rotation is typically two 2 orders of magnitude larger than in the case of poloidal rotation.

4. NUMERICAL SOLUTIONS

In order to explore further the interaction of tearing modes with a resistive shell, the equations given in Section 2 have been solved numerically.

Figure 3 gives the saturated island width for an m = 2 tearing mode as a function of $\omega\tau_v$. The current profiles are taken to have the form $j = j_o(1 - (r^2/a^2))^\nu$ with $q_o = 0.8$, and the resistive shell is at the surface of the plasma. For $q_a \gtrsim 4$, $(r_s/a \lesssim 0.7)$, the resonant surface is sufficiently far from the shell that the stabilising effect of high frequency is negligible. The reason, of course, is that even a perfectly conducting shell is ineffective in such cases. For lower q_a, the resonance is closer to the shell and the effect of high frequency is more marked. For $q_a < 2.75$ $(r_s/a > 0.85)$, the change from zero frequency to high frequency completely stabilises the mode.

The subsequent figures show the results of time-dependent calculations of mode locking for the m = 2, n = 1 mode. The current profiles are taken to have the form given above, with $q_o = 1$. It is assumed that the whole plasma rotates toroidally, so that $d\omega/dt \propto w^4$ as in the example discussed in section 3 and we take a parabolic density profile with $\rho_o = 5\times10^{-8}$ kg.m^{-3}, R = 3m, a = 1.4m, $\tau_v = 2.5(b/a)$ms, and with $Z_{eff}T^{-3/2}(keV) = 10$, $\eta = 2.8\times10^{-7}$.

First, to illustrate the general behaviour, Fig.4 shows the results for a relatively low initial frequency ω_o= 2000 rad/sec, ($\omega\tau_v = 5$), with b = a and $q_a = 4.0$. The island ultimately saturates at w = 0.16a, but the mode locking occurs for w = 0.11a. The magnetic signal, $\dot{B}_\theta$, grows initially in response to the instability. It reaches a maximum and begins to fall when the coupling to the wall starts to reduce the frequency (since $\dot{\tilde{B}} \sim \omega\tilde{B}$). The increased amplitude then strengthens the change and the frequency ω is finally reduced to zero with a strong exponential decay. This is the mode lock.

When the resonant layer is closer to the conducting shell, an abrupt increase in the island growth rate is also observed at the time of locking. This is illustrated in Fig. 5. Here we take an initial frequency of ω_o = 6000 rad/sec, ($\omega\tau_v = 15$), consistent with the frequencies of Mirnov oscillations observed in JET ohmic discharges [3]. However in order to show more clearly the effect of the vessel we keep b = a. Figure 5a shows the island width as a function of time for the two cases of $q_a = 2.5$ ($r_s/a = 0.88$) and $q_a = 4.0$ ($r_s/a = 0.68$). Abrupt changes in w can be seen in both cases, although clearly the effect is stronger the closer the resonant surface is to the wall. Figure 5b shows the corresponding frequency plots. The lock occurs earlier for the case with lower q_a.

A plot of the stability parameter $\Delta'(t)$ is shown in Fig. 6 for the case with $q_a = 4$. During the locking the real part of Δ', Δ'_R 'jumps' to a higher value, causing the changes in the island growth rates seen in Fig. 5a. This is easily understood if we express ψ as in Eq. (8) and take ψ constant over the island. Then Δ' can also be expressed in the form

$$\Delta' = \Delta'_\infty + \alpha\ (\Delta'_v - \Delta'_\infty).$$

In the example shown here, where the resonant layer is not close to the vessel, $\alpha \approx f$, thus at high frequencies $\Delta' \approx \Delta'_v$, while after the locking $\Delta' = \Delta'_\infty$. The rotation damping is proportional to the imaginary part of Δ', Δ'_I, which decays to zero during the locking.

A plot of the parameter α as a function of $\omega\tau_v$ is helpful to understand why the locking occurs earlier when the resonant layer is closer to the wall. Figure 7 shows the plots of α_R and α_I for the case of $q_a = 2.25$ for two wall positions, a) $r_s/b = 0.94$ and, b) $r_s/b = 0.72$. While for case (b) α_I has a maximum for $\omega\tau_v = 3$, for case (a) this occurs at the higher value of $\omega\tau_v = 10$. Since $d\omega/dt$ is proportional to α_I, it is clear that in the case where the resonance layer is closer to the wall, most of the frequency decay will occur at a higher frequency.

We now take the more realistic case of a wall separated from the plasma with $b = 1.2a$, $\tau_v = 3$ms and an initial frequency $\omega_o = 6000$ rad/s. Figure 8 shows how the time of locking is affected both by the effects of varying the equilibrium current density profile and the type of rotation. The time of locking is defined as the total time taken for the frequency to change from ω_o to 1% of its initial value as the mode grows from zero amplitude. As q_a is increased from 2.25 to 5, the island width at which the locking occurs varies from 0.06a to 0.09a in the poloidal case and 0.16a to 0.20a in the

toroidal case.

Figure 9 shows the time evolution of the amplitudes of the perturbed fields $\tilde{B}_\theta = |\psi'|^{1/2}$ and $\tilde{B}_r = \frac{m}{a}|\psi|^{1/2}$ at the plasma edge, r = a, for the toroidal case with $q_a = 5$ shown in Fig.8. The ratio between $\tilde{B}_\theta$ and $\tilde{B}_r$ at the plasma edge is obtained from the boundary condition (4) as

$$\tilde{B}_\theta/\tilde{B}_r = |1 + f(a/b)^{2m}|/|1 - f(a/b)^{2m}|.$$

At high frequencies this becomes

$$\frac{\tilde{B}_\theta}{\tilde{B}_r} = \frac{(b/a)^{2m} + 1}{[((b/a)^{2m} - 1)^2 + m^2/\omega^2\tau_v^2]^{1/2}}.$$

This ratio therefore depends on the wall position, such that for a wall close to the plasma $\tilde{B}_\theta/\tilde{B}_r = \frac{2}{m}\omega\tau_v$, while for a wall at infinity $\tilde{B}_\theta/\tilde{B}_r = 1$. For the particular example shown in Fig. 9, $(b/a)^{2m} = 2.1$, thus initially $m^2/\omega^2\tau_v^2 \ll ((b/a)^{2m} - 1)^2$ giving

$$\frac{\tilde{B}_\theta}{\tilde{B}_r} = \frac{(b/a)^{2m} + 1}{(b/a)^{2m} - 1} = 2.8.$$

The sudden increase in B_r illustrates further the loss of stabilisation which occurs when the mode is brought to rest. After the locking, f = 0, thus $\tilde{B}_\theta = \tilde{B}_r$ as expected from the vacuum solution.

5. DISCUSSION

The theory outlined above can clearly be extended to include further physics. If it is found that the proposed model explains the overall

behaviour, then a more detailed examination of such extensions could be rewarding.

The time dependent numerical calculations, using JET parameters, show that the model can explain in a qualitative way both the overall frequency and the radial field evolution observed from JET MHD signals [2,3]. The observed times for mode locking in JET ohmic discharges are consistent with a calculation where the island rotates in the toroidal direction and the mass involved is greater than that in the island.

In the case of toroidal motion the question of the mass involved can be treated if the transfer of momentum takes place through viscosity. Thus, instead of assuming rigid body motion the velocity distribution across the radius could be determined by solving an equation of the form

$$\frac{\partial v_\phi}{\partial t} = \frac{F_\phi(r,t)}{\rho} + \nu \frac{1}{r} \frac{\partial}{\partial r} \left(r \frac{\partial v_\phi}{\partial r} \right).$$

The resulting $v_\phi(r_s,t)$ would then give the rate of change of frequency

$$\frac{d\omega}{dt} = - \frac{n}{R} \frac{dv_\phi(r_s,t)}{dt} .$$

An investigation of this behaviour would give information on the rate of momentum transfer.

It is normally assumed that the poloidal motion is severely limited by a poloidal drag force such as predicted by neo-classical theory. However, if the momentum transfer is sufficiently fast then poloidal motion can result. The neo-classical poloidal drag is $\sim \rho \nu_i v_\theta$ where ν_i is the ion collision frequency. Thus a poloidal force of this order could lead to a significant effect. In JET, ν_i^{-1} is typically $\sim$ 1ms and since the frequency slowing

time reaches a value of similar order at large amplitudes, some poloidal motion might occur. However, comparison of the experimental results from JET ohmic discharges with Table 1 indicates that the motion is principally toroidal.

In the model presented here, the frequency is never actually brought to zero, but rather decays exponentially to very small values. It cannot therefore explain the spatial location of the locking observed in experiments. The tendency for the island to lock at a particular position as observed in JET suggests that asymmetries in the vessel or in the equilibrium fields play a role [3]. This could be taken into account by modifying the boundary condition given by Eq. (4).

The model described here involves an external cause for the slowing down of tearing modes. However, intrinsic plasma effects may also play a role. Another theory of mode slowing is based on removal of the density and temperature gradients through island formation. It has been proposed by Biskamp [8] and Scott et al. [9] that, since the frequency of small amplitude tearing modes is related to the diamagnetic frequency ω_*, the reduction of the gradients should produce a slowing of the mode with increasing amplitude, as observed. However, as remarked by Scott et al., this model could not explain why large amplitude modes are seen without significant reduction in the frequency. Furthermore, in plasmas which are "spun" by neutral beam injection to produce frequencies several times ω_*, the frequency is brought to zero (mode locking) and not just changed by ω_*.

6. SUMMARY

A theoretical model of mode-locking through the effect of a resistive shell has been described. This model has been used to obtain both analytic and numerical solutions. At high frequencies the resistive shell behaves

like a perfect conductor, but generally this does not prevent the growth of tearing modes. As the magnetic island grows there is a transfer of momentum between the plasma and the shell which reduces the frequency. This allows further penetration of the oscillating magnetic field into the shell. The reduction in frequency and the increased penetration each enhance the other, leading finally to a complete locking of the mode.

ACKNOWLEDGEMENT

The authors would like to thank Dr. E. Lazzaro for helpful discussions and Dr. D.J. Ward for drawing attention to the implications of the mode locking of spun plasmas.

REFERENCES

[1] Nave, M.F.F., Wesson, J.A., in Controlled Fusion and Plasma Physics (Proc. 14th Eur. Conf., Madrid, 1987), Vol. 11D, Part III, European Physical Society (1987) 1103.

[2] Snipes, J.A., Campbell, D.J., Haynes, P.S., Hender et al., in Controlled Fusion and Plasma Physics (Proc. 14th Eur. Conf., Madrid, 1987), Vol. 11D, Part I, European Physical Society (1987) 69.

[3] Snipes, J.A., Campbell, D.J., Haynes, P.S., et al., Nucl. Fusion 28 (1988) 1085.

[4] Rutherford, R.H., Phys. Fluids 16, (1973) 1703.

[5] Wesson, J.A. Nuc. Fus. 18, (1978) 87.

[6] White, R.B. et al. Phys. Fluids 20, (1977) 800.

[7] Berge, G., Sandal, L.K. and Wesson, J.A., Physica Scripta 40 (1989) 173.

[8] Biskamp, D., Nucl. Fusion 19, (1979) 777.

[9] Scott, B.D., Hassam, A.B. and Drake, J.F., Phys. Fluids 28 (1985) 275.

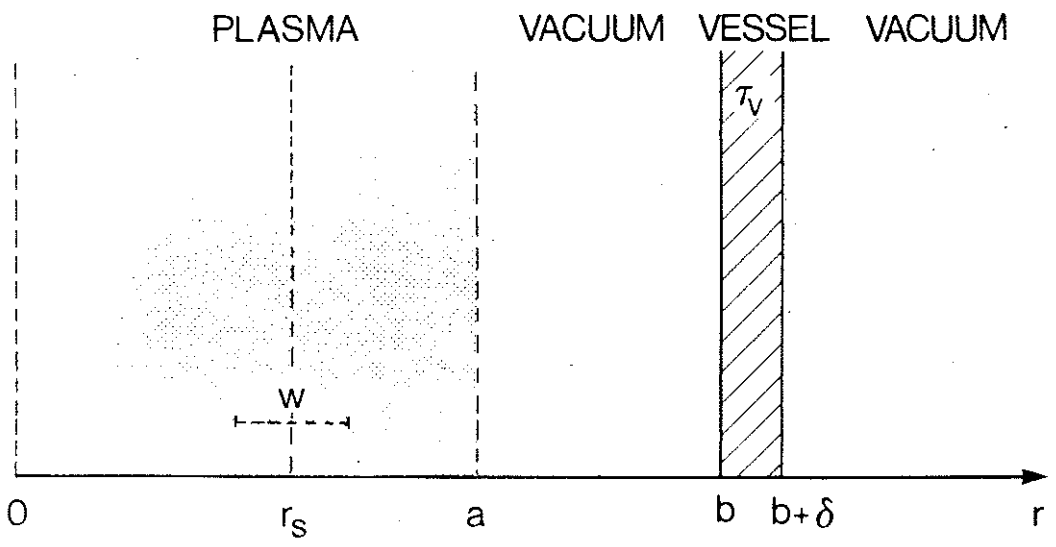

Fig. 1 Geometry of the problem

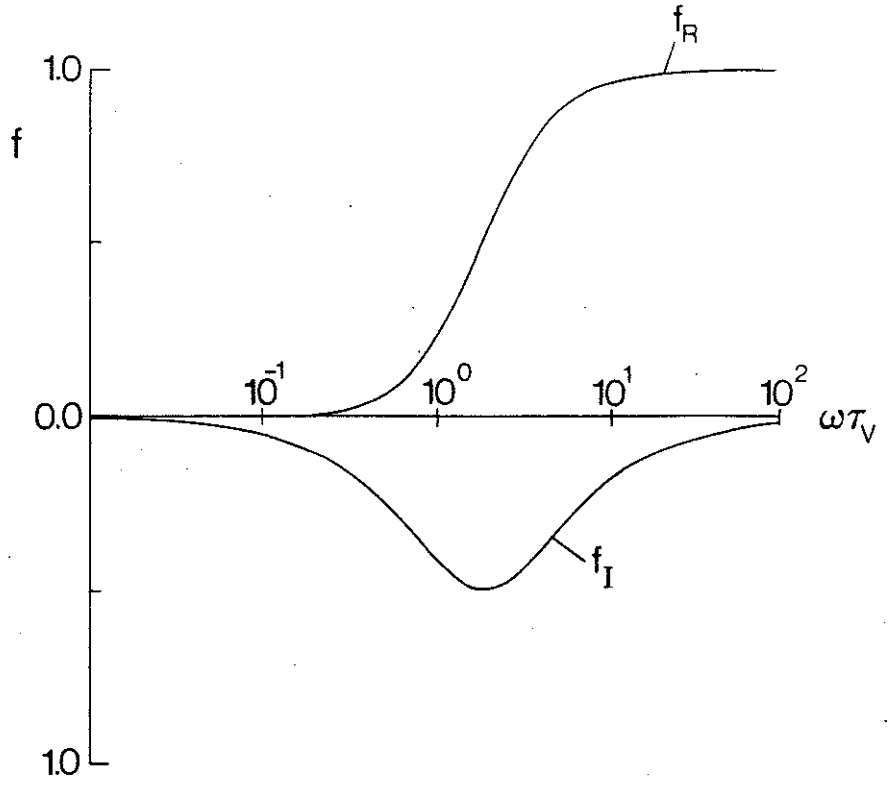

Fig. 2 Plot of the real and imaginary parts of f versus $\omega\tau_v$ for m = 2.

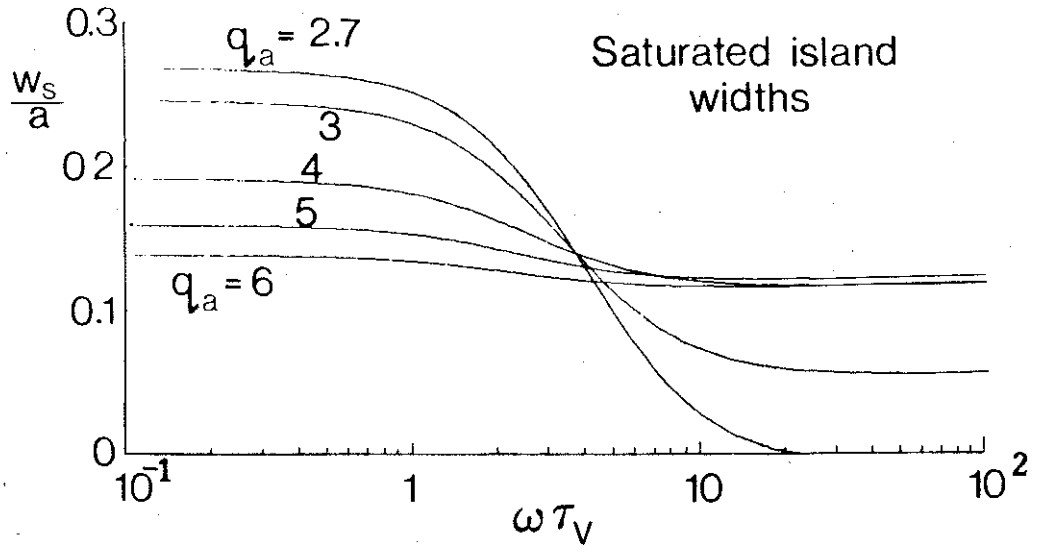

Fig. 3 Graphs of saturated m = 2 island width, w_s, against $\omega\tau_v$ for different values of q_a.

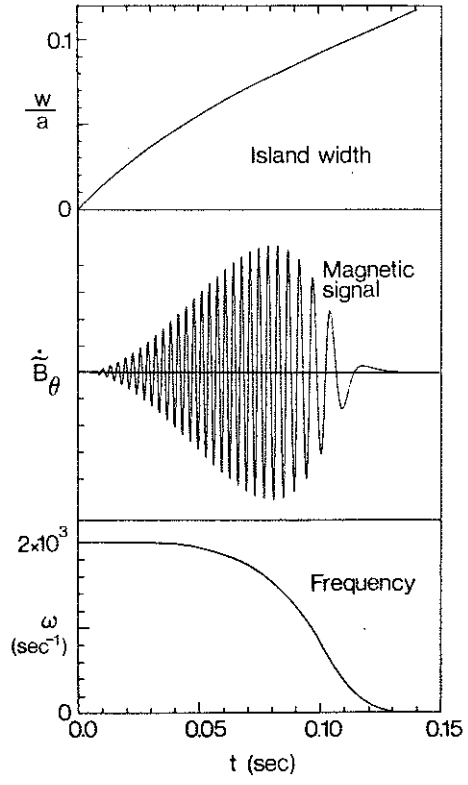

Fig. 4 General behaviour during mode-locking. Graphs show the time development of the island width w, the magnetic signal $\tilde{\dot{B}}_\theta$ and the frequency ω.

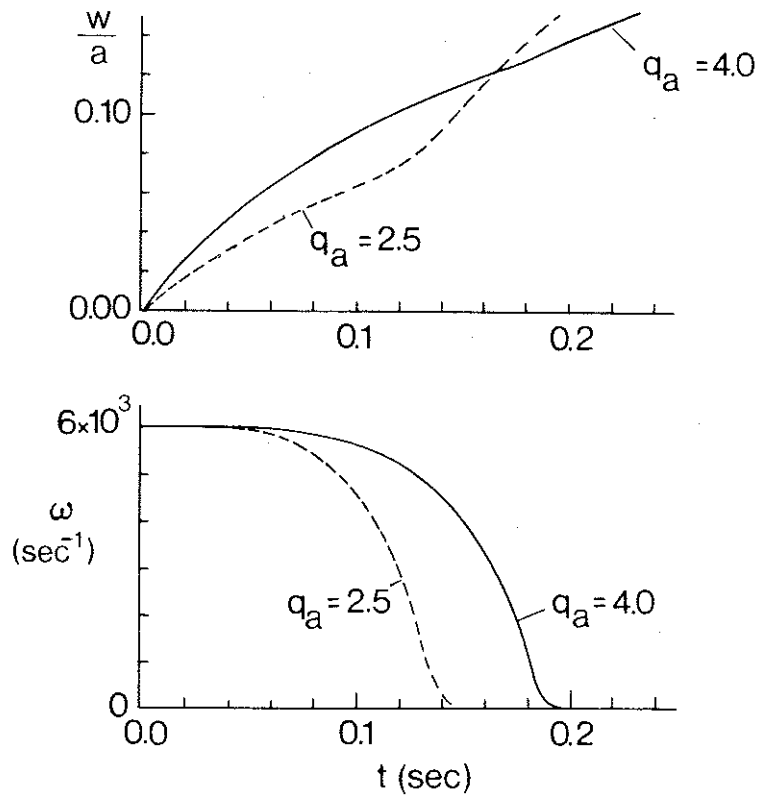

Fig. 5 Mode-locking for two values of q_a. Graphs show the time development of the island width and the frequency.

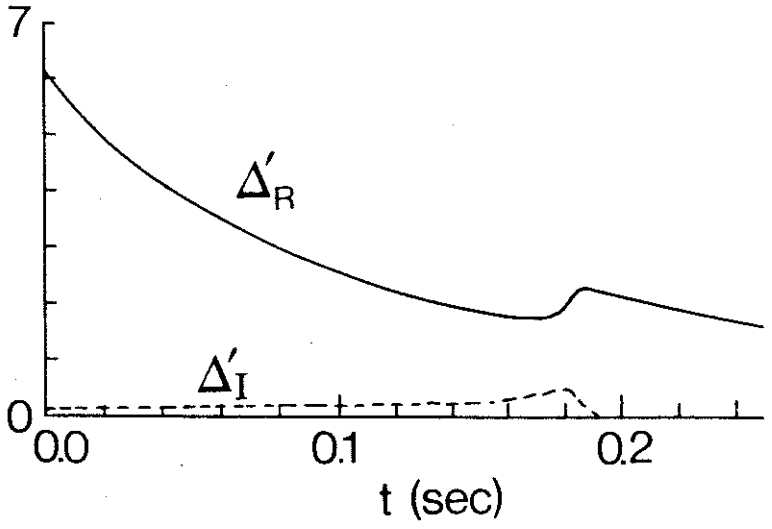

Fig. 6 Real and imaginary parts of the stability parameter Δ' for the case of $q_a = 4$.

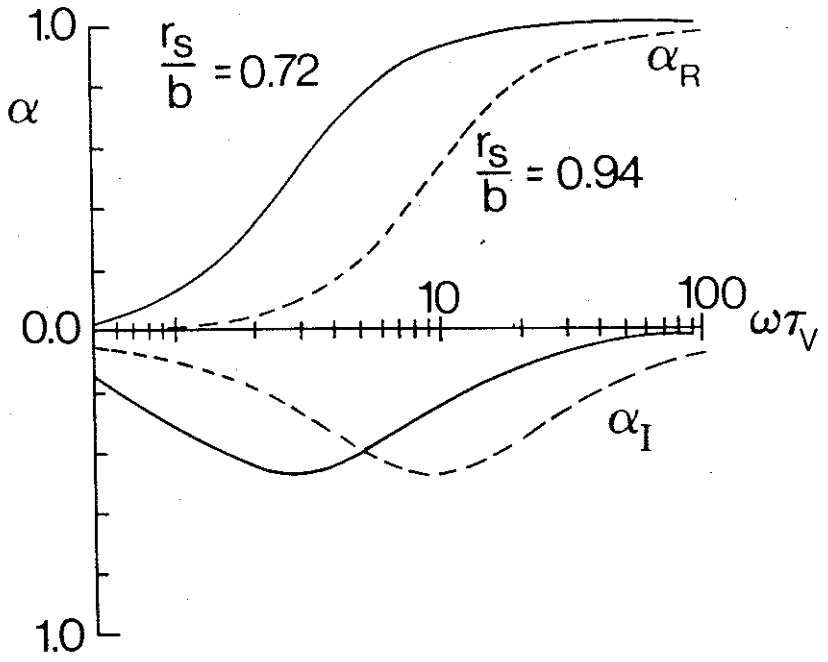

Fig. 7 The parameter α as a function of $\omega\tau_v$ for $r_s/b=0.72$ (full lines) and $r_s/b=0.94$ (dashed lines).

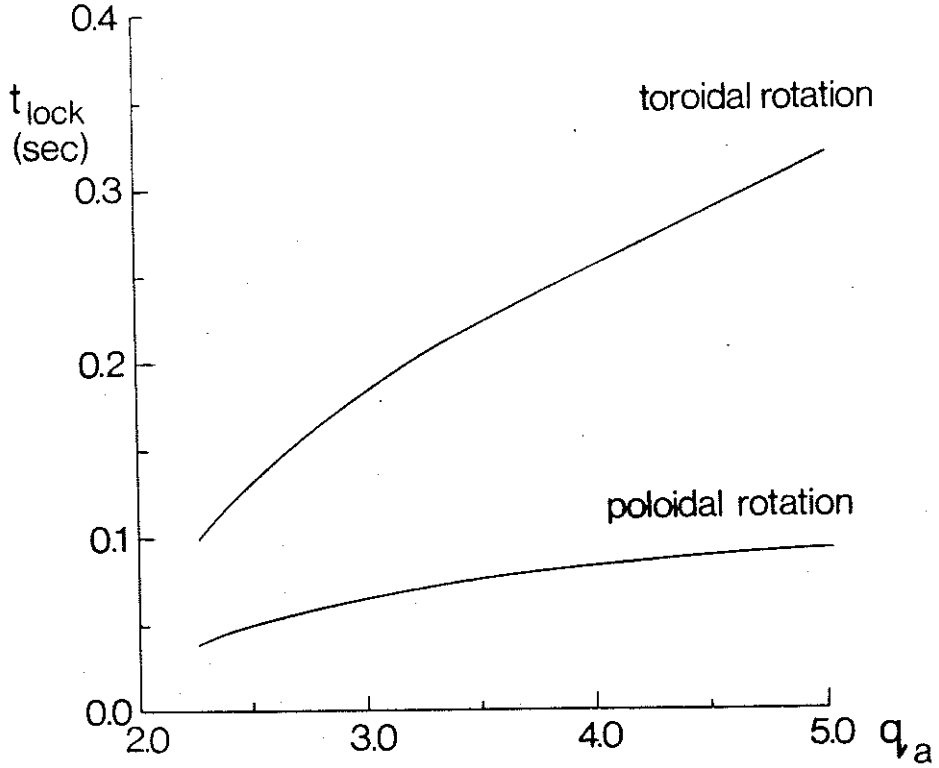

Fig. 8 Time of locking versus q_a for the cases of poloidal and toroidal rotation.

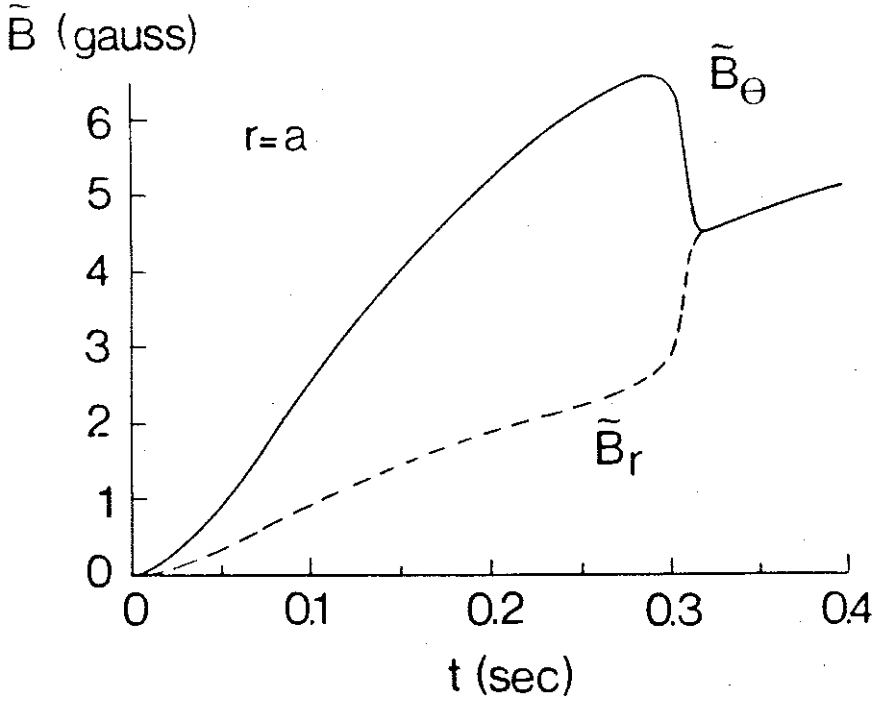

Fig. 9 The amplitudes of $\tilde{B}_r$ (a) and $\tilde{B}_\theta$ (a) as a function of time for the case of toroidal motion with $q_a = 5$.

APPENDIX 1.

THE JET TEAM

JET Joint Undertaking, Abingdon, Oxon, OX14 3EA, U.K.

J.M.Adams[1], F.Alladio[4], H.Altmann, R.J.Anderson, G.Appruzzese, W.Bailey, B.Balet, D.V.Bartlett, L.R.Baylor[24], K.Behringer, A.C.Bell, P.Bertoldi, E.Bertolini, V.Bhatnagar, R.J.Bickerton, A.Boileau[3], T.Bonicelli, S.J.Booth, G.Bosia, M.Botman, D.Boyd[31], H.Brelen, H.Brinkschulte, M.Brusati, T.Budd, M.Bures, T.Businaro[4], H.Buttgereit, D.Cacaut, C.Caldwell-Nichols, D.J.Campbell, P.Card, J.Carwardine, G.Celentano, P.Chabert[27], C.D.Challis, A.Cheetham, J.Christiansen, C.Christodoulopoulos, P.Chuilon, R.Claesen, S.Clement[30], J.P.Coad, P.Colestock[6], S.Conroy[13], M.Cooke, S.Cooper, J.G.Cordey, W.Core, S.Corti, A.E.Costley, G.Cottrell, M.Cox[7], P.Cripwell[13], F.Crisanti[4], D.Cross, H.de Blank[16], J.de Haas[16], L.de Kock, E.Deksnis, G.B.Denne, G.Deschamps, G.Devillars, K.J.Dietz, J.Dobbing, S.E.Dorling, P.G.Doyle, D.F.Düchs, H.Duquenoy, A.Edwards, J.Ehrenberg[14], T.Elevant[12], W.Engelhardt, S.K.Erents[7], L.G.Eriksonn[5], M.Evrard[2], H.Falter, D.Flory, M.Forrest[7], C.Froger, K.Fullard, M.Gadeberg[11], A.Galetsas, R.Galvao[8], A.Gibson, R.D.Gill, A.Gondhalekar, C.Gordon, G.Gorini, C.Gormezano, N.A.Gottardi, C.Gowers, B.J.Green, F.S.Griph, M.Gryzinski[26], R.Haange, G.Hammett[6], W.Han[9], C.J.Hancock, P.J.Harbour, N.C.Hawkes[7], P.Haynes[7], T.Hellsten, J.L.Hemmerich, R.Hemsworth, R.F.Herzog, K.Hirsch[14], J.Hoekzema, W.A.Houlberg[24], J.How, M.Huart, A.Hubbard, T.P.Hughes[32], M.Hugon, M.Huguet, J.Jacquinot, O.N.Jarvis, T.C.Jernigan[24], E.Joffrin, E.M.Jones, L.P.D.F.Jones, T.T.C.Jones, J.Källne, A.Kaye, B.E.Keen, M.Keilhacker, G.J.Kelly, A.Khare[15], S.Knowlton, A.Konstantellos, M.Kovanen[21], P.Kupschus, P.Lallia, J.R.Last, L.Lauro-Taroni, M.Laux[33], K.Lawson[7], E.Lazzaro, M.Lennholm, X.Litaudon, P.Lomas, M.Lorentz-Gottardi[2], C.Lowry, G.Magyar, D.Maisonnier, M.Malacarne, V.Marchese, P.Massmann, L.McCarthy[28], G.McCracken[7], P.Mendonca, P.Meriguet, P.Micozzi[4], S.F.Mills, P.Millward, S.L.Milora[24], A.Moissonnier, P.L.Mondino, D.Moreau[17], P.Morgan, H.Morsi[14], G.Murphy, M.F.Nave, M.Newman, L.Nickesson, P.Nielsen, P.Noll, W.Obert, D.O'Brien, J.O'Rourke, M.G.Pacco-Düchs, M.Pain, S.Papastergiou, D.Pasini[20], M.Paume[27], N.Peacock[7], D.Pearson[13], F.Pegoraro, M.Pick, S.Pitcher[7], J.Plancoulaine, J-P.Poffé, F.Porcelli, R.Prentice, T.Raimondi, J.Ramette[17], J.M.Rax[27], C.Raymond, P-H.Rebut, J.Removille, F.Rimini, D.Robinson[7], A.Rolfe, R.T.Ross, L.Rossi, G.Rupprecht[14], R.Rushton, P.Rutter, H.C.Sack, G.Sadler, N.Salmon[13], H.Salzmann[14], A.Santagiustina, D.Schissel[25], P.H.Schild, M.Schmid, G.Schmidt[6], R.L.Shaw, A.Sibley, R.Simonini, J.Sips[16], P.Smeulders, J.Snipes, S.Sommers, L.Sonnerup, K.Sonnenberg, M.Stamp, P.Stangeby[19], D.Start, C.A.Steed, D.Stork, P.E.Stott, T.E.Stringer, D.Stubberfield, T.Sugie[18], D.Summers, H.Summers[20], J.Taboda-Duarte[22], J.Tagle[30], H.Tamnen, A.Tanga, A.Taroni, C.Tebaldi[23], A.Tesini, P.R.Thomas, E.Thompson, K.Thomsen[11], P.Trevalion, M.Tschudin, B.Tubbing, K.Uchino[29], E.Usselmann, H.van der Beken, M.von Hellermann, T.Wade, C.Walker, B.A.Wallander, M.Walravens, K.Walter, D.Ward, M.L.Watkins, J.Wesson, D.H.Wheeler, J.Wilks, U.Willen[12], D.Wilson, T.Winkel, C.Woodward, M.Wykes, I.D.Young, L.Zannelli, M.Zarnstorff[6], D.Zasche[14], J.W.Zwart.

PERMANENT ADDRESS

1. UKAEA, Harwell, Oxon. UK.
2. EUR-EB Association, LPP-ERM/KMS, B-1040 Brussels, Belgium.
3. Institute National des Récherches Scientifique, Quebec, Canada.
4. ENEA-CENTRO Di Frascati, I-00044 Frascati, Roma, Italy.
5. Chalmers University of Technology, Göteborg, Sweden.
6. Princeton Plasma Physics Laboratory, New Jersey, USA.
7. UKAEA Culham Laboratory, Abingdon, Oxon. UK.
8. Plasma Physics Laboratory, Space Research Institute, Sao José dos Campos, Brazil.
9. Institute of Mathematics, University of Oxford, UK.
10. CRPP/EPFL, 21 Avenue des Bains, CH-1007 Lausanne, Switzerland.
11. Risø National Laboratory, DK-4000 Roskilde, Denmark.
12. Swedish Energy Research Commission, S-10072 Stockholm, Sweden.
13. Imperial College of Science and Technology, University of London, UK.
14. Max Planck Institut für Plasmaphysik, D-8046 Garching bei München, FRG.
15. Institute for Plasma Research, Gandhinagar Bhat Gujat, India.
16. FOM Instituut voor Plasmafysica, 3430 Be Nieuwegein, The Netherlands.
17. Commissiariat à L'Energie Atomique, F-92260 Fontenay-aux-Roses, France.
18. JAERI, Tokai Research Establishment, Tokai-Mura, Naka-Gun, Japan.
19. Institute for Aerospace Studies, University of Toronto, Downsview, Ontario, Canada.
20. University of Strathclyde, Glasgow, G4 ONG, U.K.
21. Nuclear Engineering Laboratory, Lapeenranta University, Finland.
22. JNICT, Lisboa, Portugal.
23. Department of Mathematics, Univeristy of Bologna, Italy.
24. Oak Ridge National Laboratory, Oak Ridge, Tenn., USA.
25. G.A. Technologies, San Diego, California, USA.
26. Institute for Nuclear Studies, Swierk, Poland.
27. Commissiariat à l'Energie Atomique, Cadarache, France.
28. School of Physical Sciences, Flinders University of South Australia, South Australia SO42.
29. Kyushi University, Kasagu Fukuoka, Japan.
30. Centro de Investigaciones Energeticas Medioambientales y Techalogicas, Spain.
31. University of Maryland, College Park, Maryland, USA.
32. University of Essex, Colchester, UK.
33. Akademie de Wissenschaften, Berlin, DDR.

CR 88.49.1A